Available online at www.sciencedirect.com
SCIENCE DIRECT®
Surface Science 540 (2003) 39–54
SURFACE SCIENCE
www.elsevier.com/locate/susc

Structural study of adsorption of isonicotinic acid and related molecules on rutile $TiO_2(1\,1\,0)$ I: XAS and STM

J. Schnadt [a,*], J. Schiessling [a], J.N. O'Shea [a,1], S.M. Gray [b], L. Patthey [d], M.K.-J. Johansson [c], M. Shi [d], J. Krempaský [d], J. Åhlund [a], P.G. Karlsson [a], P. Persson [a], N. Mårtensson [a,2], P.A. Brühwiler [a,3]

[a] *Department of Physics, Uppsala University, Box 530, 751 21 Uppsala, Sweden*
[b] *Department of Synchrotron Radiation Research, University of Lund, Box 118, 221 00 Lund, Sweden*
[c] *Division of Solid State Physics/the Nanometer Consortium, University of Lund, Box 118, 221 00 Lund, Sweden*
[d] *Swiss Light Source, Paul Scherrer Institut, 5232 Villigen-PSI, Switzerland*

Received 21 February 2003; accepted for publication 9 June 2003

Abstract

X-ray absorption spectroscopy (XAS) and scanning tunneling microscopy (STM) have been used to study the absorption of monolayers of the pyridinecarboxylic acid monomers (isonicotinic acid, nicotinic acid, and picolinic acid) and benzoic acid on a rutile $TiO_2(1\,1\,0)$ surface. We find that the pyridine and phenyl rings are oriented with their planes largely perpendicular to the surface. The azimuthal orientations are strongly influenced by adsorbate–adsorbate interactions, which in each case leads to at least two different molecular species. In order to reach this conclusion a detailed strategy has been developed for the interpretation of angle-dependent XAS data, which does not rely on any curve fitting procedures.

Keywords: X-ray absorption spectroscopy; Scanning tunneling microscopy; Chemisorption; Evaporation and sublimation; Aromatics; Titanium oxide; Single crystal surfaces

1. Introduction

The pyridinecarboxylic acid monomers and benzoic acid (see Fig. 1) are biologically and technologically important molecules. They play roles as diverse as reaction partners in industrial processes [1] (partly as contaminants in photocatalytic processes [2–4], partly as desired intermediates or educts [5–9]), building blocks in photovoltaic devices [10], food preservatives [1], and as model systems in environmental studies [11].

* Corresponding author. Present address: Department of Physics and Astronomy, University of Aarhus, Ny Munkegade, 8000 Aarhus C, Denmark. Tel.: +45-8942-3769; fax: +45-8612-0740.
E-mail addresses: achim@phys.au.dk (J. Schnadt), paul.bruehwiler@empa.ch (P.A. Brühwiler).
[1] Present address: School of Physics and Astronomy, University of Nottingham, Nottingham, NG7 2RD, United Kingdom.
[2] Also at MAX-Lab, University of Lund, Box 118, 221 00 Lund, Sweden.
[3] Present address: EMPA, Lerchenfeldstr. 5, 9014 St. Gallen, Switzerland.

0039-6028/$ - see front matter © 2003 Elsevier B.V. All rights reserved.
doi:10.1016/S0039-6028(03)00827-6

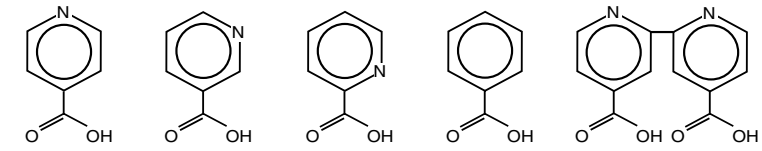

Fig. 1. Schematic structures of the pyridine-carboxylic acid isomers, benzoic acid, and bi-isonicotinic acid. Unspecified vertices represent either C atoms or C atoms with associated H atoms. For isonicotinic acid the N atom is in the para position relative to the carboxylic group, for nicotinic acid in the meta position, and for picolinic acid in the ortho position.

Furthermore, nicotinic acid is vitamin B3 [1]. In many of the mentioned applications and environments surfaces and surface reactions play an important role, especially in the field of catalysis. Nevertheless, only a few surface science studies have been concerned with the interaction of benzoic acid with metal surfaces [12–29] and even fewer using oxide surfaces [30–35]. To our knowledge, no UHV (ultrahigh vacuum) adsorption study has been performed for the pyridinecarboxylic monomers using in situ prepared samples, in contrast to the situation for the isonicotic acid dimer, bi-isonicotinic acid, whose adsorption on rutile [36–40] and anatase [41,42] TiO_2 has been treated in quite some detail. More information has been reported, however, for the adsorption of the monomer molecules on metal surfaces in solution and then investigated either in UHV or in solution [43–48].

Following initial UHV studies of the pyridinecarboxylic acid monomers concerned with the formation of hydrogen bonds in in situ grown multilayers [49,50], the present article is the first of two that treat the structural aspects of the adsorption of monolayers of the pyridinecarboxylic acid monomers and benzoic acid on rutile $TiO_2(1\,1\,0)$ under UHV conditions (the companion paper [51] will be referred to as "II"). II is devoted to the photoemission spectroscopy results, which provide information on the molecule-substrate bond, and the intermolecular interactions. Here we present the results of X-ray absorption spectroscopy (XAS) and scanning tunneling microscopy (STM) experiments in order to determine the fundamentals of the adsorption geometry, in particular the orientations of the pyridine and phenyl rings.

2. Experimental and theoretical

The XAS experiments were performed at beamlimes I511 [52] and D1011 [53,54] at the Swedish national synchrotron radiation facility MAX-Lab in Lund. The STM was conducted at the UHV-STM [55] laboratory at the Department of Synchrotron Radiation Research in Lund. The base pressure was in the low 10^{-10} Torr range for the preparation chambers and in the low 10^{-11} range for the analysis chambers. The $TiO_2(1\,1\,0)$ single crystal substrates, purchased from Djévahirdjian, Industrie de Pierre Scientifique in Monthey, Switzerland, and from MaTecK, Jülich, Germany, had been annealed in 1×10^{-6} Torr O_2 at high temperatures (700 °C) in order to make them conducting by the introduction of bulk defects. The surface was then prepared [36] by cycles of repeated Ar sputtering and annealing in a 1×10^{-6} Torr oxygen (99.999%) atmosphere at temperatures between 570 and 700 °C. For the X-ray absorption measurements a home-built sample holder was used that allowed a 0–90° rotation of the sample azimuth. The chemicals were obtained from Sigma-Aldrich with a guaranteed purity > 99% (nicotinic acid > 98%) and were thoroughly outgassed in vacuum before use. They were deposited in situ [36] using a retractable and separately pumped home-built thermal evaporator with pressure and temperature monitors. The powder temperature during sublimation varied from room temperature (picolinic and benzoic

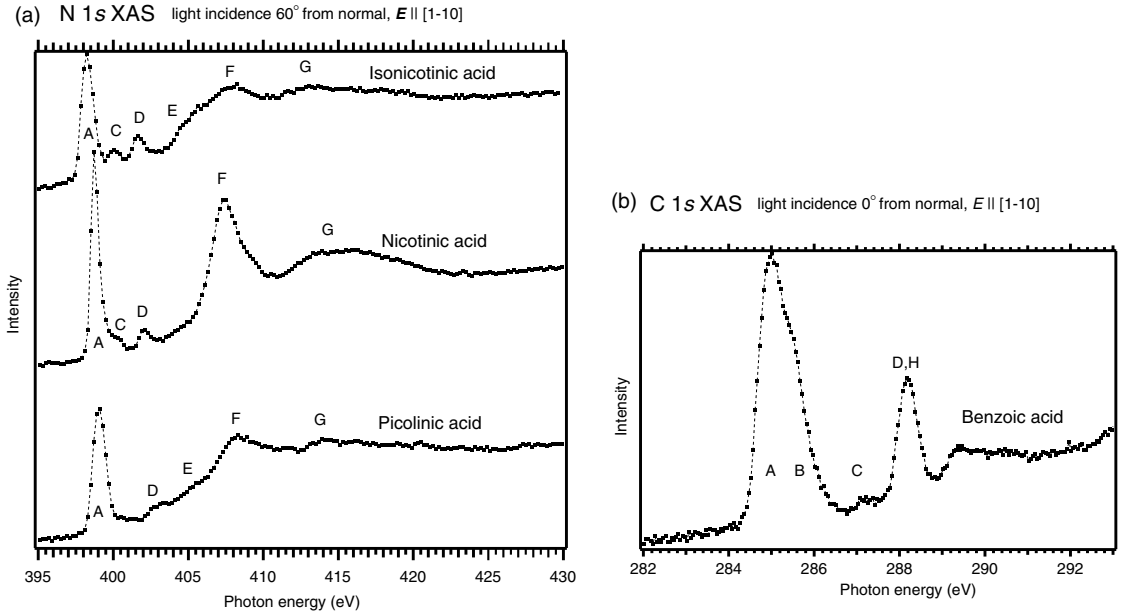

Fig. 2. N 1s X-ray absorption spectra for the pyridinecarboxylic acids and C 1s XAS for benzoic acid adsorbed on rutile TiO_2(1 1 0). The polarisation direction of the light is indicated, and the particular incidence angle chosen here highlights the existence of three low energy resonances for isonicotinic and nicotinic acid. The benzoic acid spectrum has been corrected for a varied second-order background, while a correction of the first-order throughput was not undertaken due to the insignificance of carbon contamination losses in this particular case [57].

acids) to approximately 65–90 °C for isonicotinic and nicotinic acid. The substrate was kept at 200 °C. [4] The pressure exerted by the molecules in the preparation chamber lay in the 10^{-9} Torr range, except when indicated otherwise. In this manner the TiO_2 surface was saturated with a monolayer of molecules. That no more than one layer of molecules was formed was checked by O 1s XPS (see part II).

The X-ray absorption energies were calibrated by determining the kinetic energy difference of photoemission spectra in first and second order at a relevant photon energy (typically that of the primary resonance), and utilising the extremely high reproducibility of the monochromators. A constant background was removed from the N 1s X-ray absorption spectra that was determined at photon energies a few eV below threshold. The intensity was then adjusted by normalising to the height of the step edge recorded approximately 25 eV above threshold. This procedure for intensity normalisation is valid in the case of a linear background [56]. The C 1s edge utilised in the measurements on benzoic acid is more difficult to treat as the background is highly varied [57]. The variations stem mainly from beamline-induced changes in second-order throughput and to a minor extent from losses in the first order light intensity due to carbon contamination on the optical elements. The step normalisation procedure is still applicable. In this case, if the background is sufficiently linear in the resonance region, the integrated resonance intensities obtained at different

[4] In their work on monolayers of benzoic acid on TiO_2 Guo et al. [32,33] had kept the sample at room temperature during deposition. Multilayers were not formed under these conditions. In contrast, in the present experiments the sample temperature during deposition was 200 °C. This allowed us to exclude any multilayer formation which could have occurred for isonicotinic acid and nicotinic acid (cf. the sublimating temperatures). An additional benefit was the consistency of the preparation method for monolayers of all four different molecules as well as bi-isonicotinic acid in previous investigations [36,38,39].

light incidence angles can still be compared to each other, although they do not represent the true absorption cross sections.

The incidence angle-dependence of the X-ray absorption intensities was determined by measuring the area below the corresponding peaks in the XAS after removal of a linear background. This procedure gives results consistent with a procedure in which the peak height was used instead. In the case of benzoic acid the first resonances (peaks A and B in Fig. 2) lie too close together for separate intensity measurements. Therefore the two peaks were summed together after carefully checking that they exhibit identical angle dependencies individually as judged from the lineshape.

Supporting DFT calculations were performed for gas phase monomers and dimers of isonicotinic acid using the GAUSSIAN98 [58] program with the B3LYP hybrid functional. Geometries were optimised with the 6-31G* basis set, and energies subsequently calculated with the 6-311 + G(d,p) basis set.

3. Results

3.1. X-ray absorption—pyridine and phenyl ring orientations

The main focus of the X-ray absorption investigation presented here will be to examine the orientation of the molecular pyridine (pyridinecarboxylic acids) and phenyl (benzoic acid) ring planes with respect to the $TiO_2(1\,1\,0)$ surface. In principle, the orientation can be determined from the intensity variation of both the π^* and the σ^* resonances with light incidence angle [56], while it is more convenient and more accurate to use the narrower low-lying π^*-resonances. Before discussing the angular dependence of these states in detail, we will assign the observed resonances.

In Fig. 2 the N 1s X-ray absorption spectra of the pyridinecarboxylic acid monolayers as well as the C 1s X-ray absorption spectrum of benzoic acid are shown. Resonances A, B, D, and E have π^*-character as judged from the angle-dependent measurements and the principal assignment of the lowest-lying resonance A (see below for the angle-resolved intensities of peaks A, B, and D and for the assignment of A). F and G are σ^* shape resonances [56]. C shows an angle-dependence that is characteristic of σ^*-resonances (see below and Fig. 4), and thus cannot have the same origin as peak B of the benzoic acid spectrum. Peak A corresponds to the N $1s \rightarrow 1\pi^*(b_1)$ and phenyl C $1s \rightarrow 1\pi^*(b_1)$ transitions. We attribute B to the phenyl C $1s \rightarrow \pi^*(a_2)$ excitation, which is observed in neither the N 1s spectra of the pyrdinecarboxylic acid molecules nor very clearly in the C 1s spectra of benzene [59]. In these cases the transition is dipole-forbidden, which is no longer the case for the meta and ortho carbon atoms of benzoic acid. This interpretation agrees with the observation of resonance B as a shoulder in the C 1s X-ray absorption spectra of pyridine [60]. The origin of resonance C is somewhat unclear since no calculation to-date has predicted any σ^*-like resonance with weight on the N atom in this energy region. For the pyridinecarboxylic acids we assign it tentatively to a N–H resonance caused by the nearest-neighbour molecular interaction not included in such calculations (see discussion below). Similarly, C–H resonances are observed in the C *K*-edge spectra of hydrocarbons [56], and for benzoic acid resonance C is ascribed to such a C–H resonance. The resonance is not clearly observed for picolinic acid, but it might either be contained in resonance A, following the trend seen for isonicotinic acid and nicotinic acid for it to move closer to that peak, or it might be very weak. D is assigned to the N $1s \rightarrow 3\pi^*(b_1)$ and C $1s \rightarrow 3\pi^*(b_1)$ transitions. For the C 1s spectrum the large intensity of the peak can be explained by the carboxyl C $1s \rightarrow 1\pi^*(b_1)$ excitation [23] that has been labelled H. In addition to the low-lying resonances, two σ^* resonances are observed at around 408 eV and 415 eV, though they are clearly most pronounced for nicotinic acid.

The spectra shown form part of a series of angle-resolved XAS measurements, in which the incidence angle of the incoming radiation θ as well as the sample azimuth ω with respect to the main component of the polarisation of the light were varied ($\omega = 0°, 45°, 90°$; $0° \leqslant \theta \leqslant 90°$ for θ measured from the surface normal, see Fig. 3). The results of an integration of the resonance intensi-

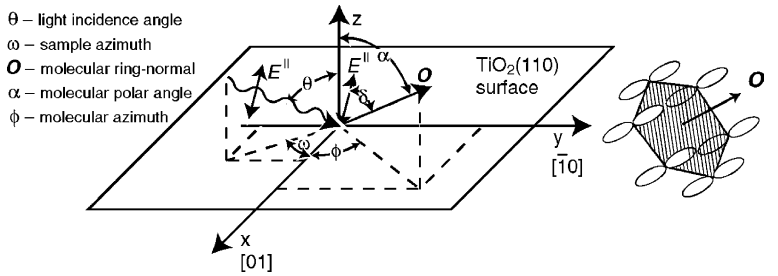

Fig. 3. Experimental geometry of the X-ray absorption measurements. The surface unit vectors $[\bar{1}\,0]$ and $[0\,1]$ correspond to the bulk $[\bar{1}\,1\,0]$ and $[0\,0\,1]$ vectors, respectively. The main component of the polarisation, indicated in the figure, lies in the plane defined by the z-axis and the projection of the incoming light onto the surface, i.e. for a sample azimuth $\omega = 0°$ it is parallel to the $[0\,1]$ direction of the surface. The molecular plane is represented by a vector $\boldsymbol{O}$ normal to the ring plane as illustrated in the right-hand panel. Here, a π^*-orbital has been symbolised by the atomic p-orbitals. α is measured between the surface normal and $\boldsymbol{O}$. δ is the angle between the polarisation and $\boldsymbol{O}$. For perfect linear polarisation the intensity of the π-resonances scales with $\cos\delta$. Expressing δ in terms of α, ϕ, θ, and ω leads to Eq. (1).

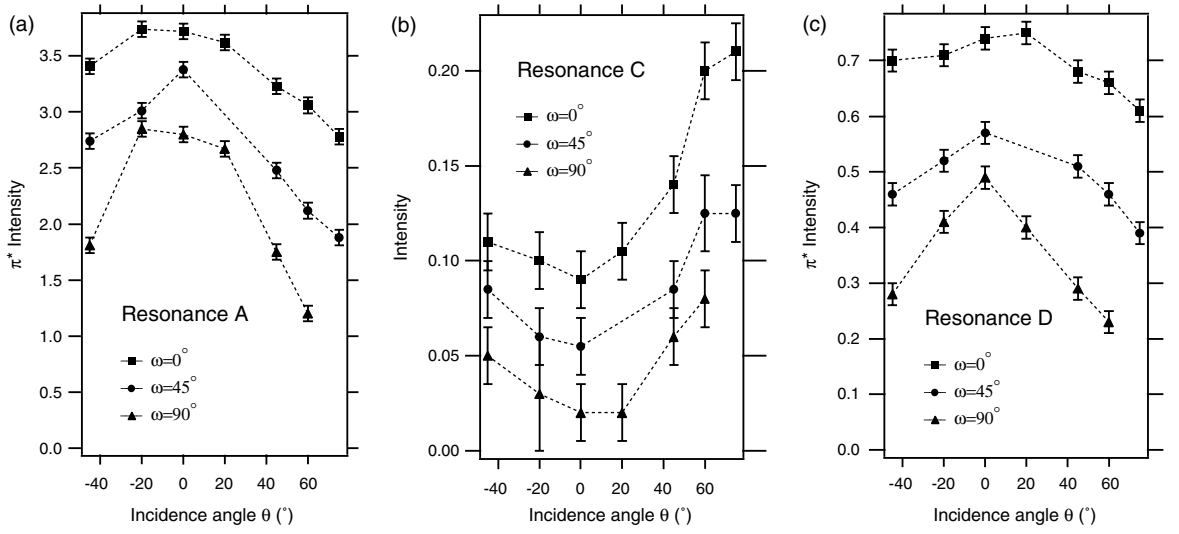

Fig. 4. Integrated X-ray absorption intensities for isonicotinic acid for the indicated resonances. For a definition of angles see Fig. 3. Offsets were applied for a clearer presentation (Resonance A: +1 ($\omega = 45°$), +2 ($\omega = 0°$); Resonance C: +0.045 ($\omega = 45°$), +0.09 ($\omega = 0°$); Resonance D: +0.3 ($\omega = 45°$), +0.5 ($\omega = 0°$)).

ties are summarised in Fig. 4 for isonicotinic acid and Fig. 5 for benzoic acid. The behaviour is qualitatively the same for nicotinic and picolinic acid and the graphs have been omitted here.

The variation of the resonance intensities in Figs. 4 and 5 with both the incidence angle of the light θ and the sample azimuth ω shows unambiguously that the molecular overlayer assumes some degree of order. The principal shape of these curves with maximum intensity at $\theta = 0°$ shows that (the majority of) the molecules stand upright with an angle of less than 45° between the pyridine/phenyl ring plane and the surface normal. The dependence of the signal on ω is clear evidence that the orientation of the pyridine and phenyl rings cannot be completely random, since that would average out any ω-dependence. The pyridine/phenyl ring orientations realised in the monolayer film are thus confined to limited ranges of ϕ.

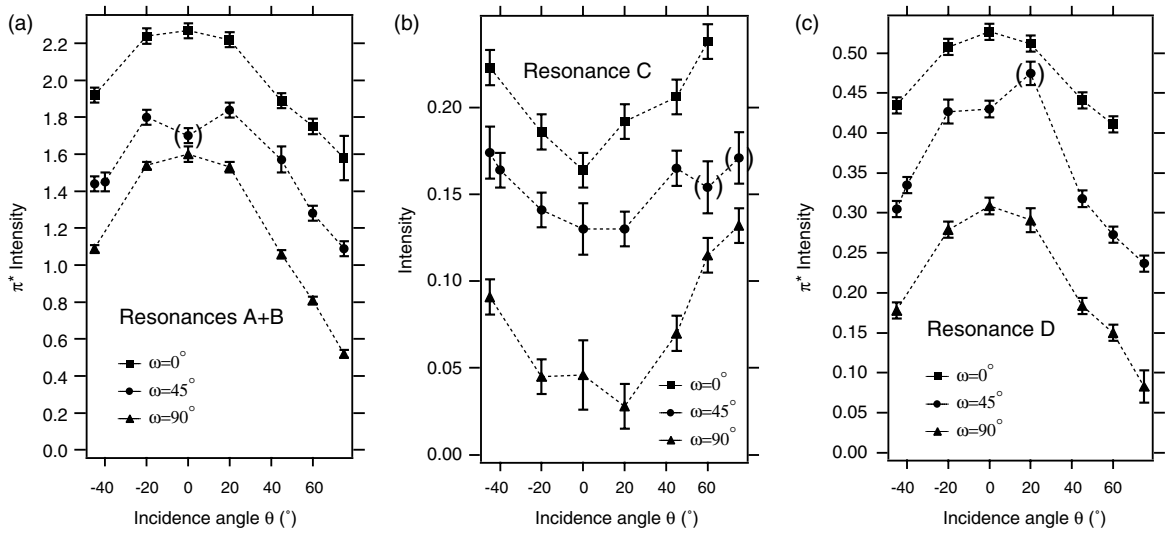

Fig. 5. Integrated XAS absorption intensities for benzoic acid. Offsets were applied for a clearer presentation (Resonances A + B: +0.5 ($\omega = 45°$), +1.0 ($\omega = 0°$); Resonance C: +0.06 ($\omega = 45°$), +0.12 ($\omega = 0°$); Resonance D: +0.15 ($\omega = 45°$), +0.3 ($\omega = 0°$)).

In the following we will further investigate this finding, focussing on the π^* resonances A/B and D. The dependence of the observed intensity variation on the light incidence angle will be analysed by considering two possibilities for the molecular geometries: (1) one molecular species, i.e., all molecules have the same orientation, and (2) two distinct molecular species that differ from each other in the set of molecular angles. We will demonstrate the feasibility of the latter possibility while the former can be excluded.

3.1.1. Modelling the XAS-data assuming a single molecular species

In the case of a single aromatic species on a twofold symmetric surface the observed π^* intensity variation with light incidence angle is described by [56]

$$I(\theta,\omega) = C(0.97\{\cos^2(90°-\theta)\cos^2\alpha + \sin^2(90°-\theta)\sin^2\alpha\cos^2(\phi-\omega)\} + 0.03\{\sin^2\alpha\sin^2(\phi-\omega)\}). \quad (1)$$

A linear polarisation factor $P = 0.97$ has been adopted based on measurements taken shortly before the present ones. θ is the incidence angle of the light, defined from the surface normal, ω is the sample azimuth, and α and ϕ are the tilt and azimuth angles of the molecule; see Fig. 3 for a definition. C is a factor related to the angle-integrated X-ray absorption cross section. For illustrational purposes $I(\theta,\omega)$ has been plotted in Fig. 6(a) for an arbitrarily chosen set of parameters $\{C,\alpha,\phi\}$. A more general inspection by means of differential calculus shows that, for α and ϕ both different from 0° to 90°, I has extremal points for $\theta = 0°$ and $\theta = 90°$, varies monotonically in between, and is point-symmetrical around $\pm 45°$ for $0° \leqslant \theta \leqslant 90°$ and $-90° \leqslant \theta \leqslant 0°$, respectively. Moreover, the first derivative $\mathrm{d}I(\theta,\omega)/\mathrm{d}\theta$ parameterises in the form $\cos\theta\sin\theta \times f(\alpha,\phi,\omega)$ where f is a function of α, ϕ, and ω, but not θ. This implies that, when plotting I as a function of θ, it always assumes the same shape, only stretched by an amplitude factor.

One can now easily derive an expression for the amplitude $A(\omega) = (I(0°,\omega) - I(90°,\omega))/2$ and from this expressions for the ratios $A(0°)/A(45°)$ and $A(0°)/A(90°)$, thus eliminating the factor C which is related to the angle-integrated X-ray absorption cross section and is thus the same for all measurements for a particular molecule. Curves of these theoretical ratios as a function of the molecular azimuth ϕ and with the tilt angle α as a parameter are given in Fig. 7. The straight lines

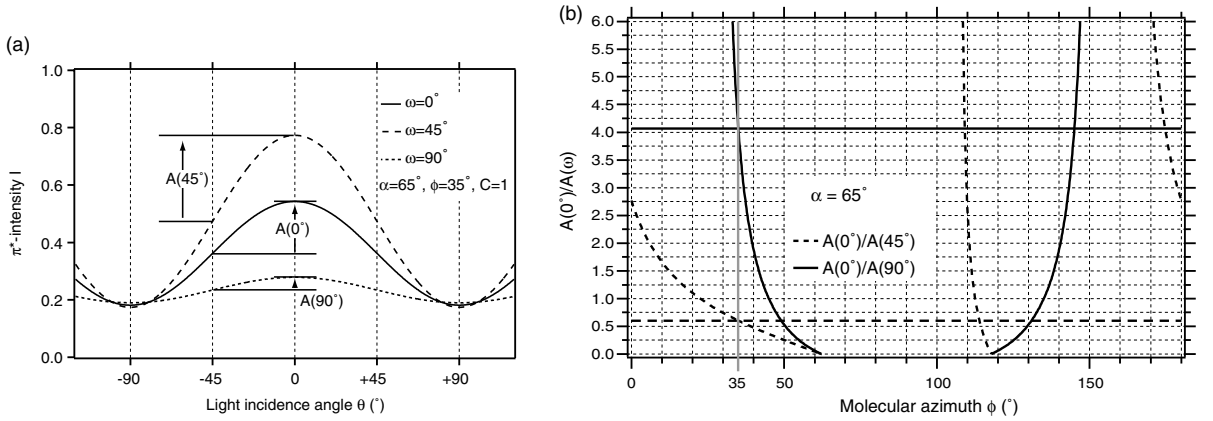

Fig. 6. (a) Plot of $I(\theta,\omega)$ for an arbitrarily chosen set of parameters $\alpha = 65°$, $\phi = 35°$, $C = 1$. The amplitudes $A(\omega)$ are indicated. (b) Amplitude ratios $A(0°)/A(45°)$ and $A(0°)/A(90°)$ for the molecular angles of panel (a). The straight horizontal lines indicate the experimental values one would obtain for this particular geometry, and the vertical grey line indicates the crossing points of these experimental lines with the amplitude ratio curves.

represent the experimental values for the A resonance of isonicotinic acid, while the hatched areas indicate the error margins of the experimental values (± 0.05). These values have been extracted from the data in Fig. 4(a) by fitting a curve of the form of Eq. (1) to the data, and requiring that it passes through at least 2/3 of the given error margins. For isonicotinic acid we find $A_{\mathrm{exp}}(0°)/A_{\mathrm{exp}}(45°) = 0.60$ and $A_{\mathrm{exp}}(0°)/A_{\mathrm{exp}}(90°) = 0.45$. Corresponding values are reported for all pyridinecarboxylic acids and benzoic acid in Table 1.

If the assumptions about the (here uniform) molecular geometry were correct, these experimental (straight) lines should cross curves with the same α parameter for the same molecular azimuth ϕ (i.e., the dashed line should cross a dashed curve and the solid line a solid curve at the same abscissa and within the same panel). Such a case is illustrated in Fig. 6(b) for the arbitrary set of molecular angles $\{\alpha,\phi\}$ of Fig. 6(a). However, none of the panels in Fig. 7 contains such a pair of curves $\{A(0°)/A(45°), A(0°)/A(90°)\}$ which matches this requirement, and, moreover, there is no angle α with $45° \leqslant \alpha \leqslant 90°$, for which this condition is fulfilled. This is concluded from the continual development of the amplitude ratio curves between $\alpha = 45°$ and $\alpha = 90°$ and a comparison to the experimental values. Since the principal form of $I(\theta,\omega)$ with a maximum for $\theta = 0°$ for the discussed resonances A and D (cf. Fig. 4(a) and (c)) demands that $\alpha > 45°$, this analysis shows that the experimental values for the amplitude ratios cannot be explained within a model that allows only a single orientation of the pyridine ring (the same is true for a model including two different orientations which are equivalent due to the twofold substrate symmetry, since a domain formation is already taken into account by Eq. (1)). Thus a pure monomer model fails in the description of the observed angular dependence of the XAS intensities for isonicotinic acid. An inspection of the experimental values for the other molecules on $TiO_2(1\,1\,0)$, cf. Table 1, yields the same finding.

3.1.2. Modelling the XAS-data assuming two distinct moleculear species

We therefore investigated if a dimer geometry, which is the next-simplest possibility, could be consistent with the X-ray absorption data. For benzoic acid (C_6H_5COOH) on $TiO_2(1\,1\,0)$ it has recently been found [32,33] that dimer formation in the [10] surface direction takes place, with dimer rows forming along the [0 1] direction, and it has been proposed that the two molecules of a dimer interact in a 'T' type manner with the difference angle between the two molecular azimuths at around 90°. We assume that benzoic acid and the pyridinecarboxylic acids, especially isonicotinic

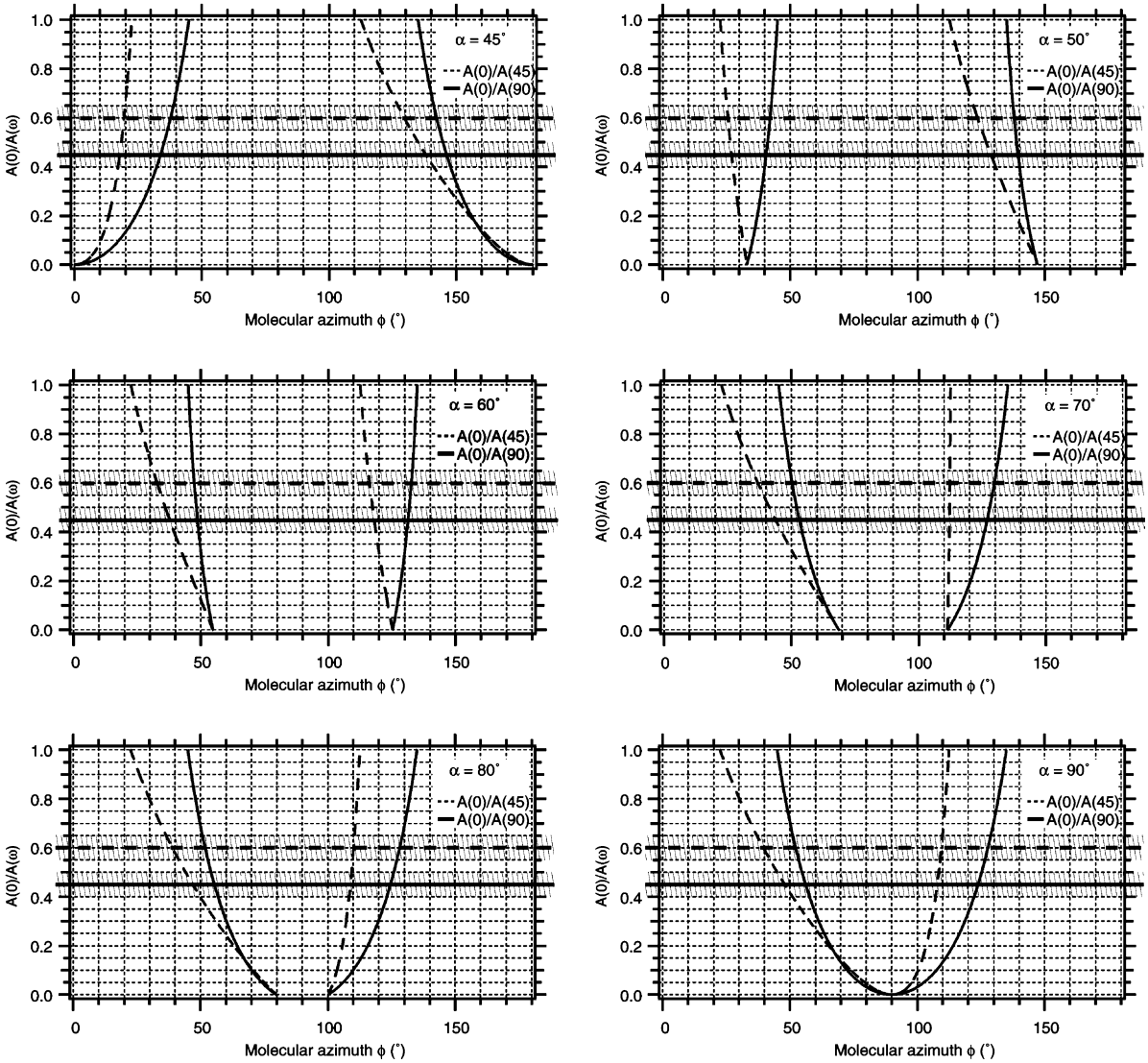

Fig. 7. Theoretical amplitude ratios $A(0°)/A(45°)$ and $A(0°)/A(90°)$ for an adsorbed planar monomer. The y-axis has been confined to values between 0 and 1 relevant to the experimental values. While the x-axis shows the molecular azimuth, the molecular polar angle is given as a parameter for the different curves. The horizontal lines give the experimental values with the hatched area indicating the experimentally derived uncertainties.

acid, will likely exhibit a similar behaviour regarding a ring interaction between neighbouring molecules. The STM experiments presented below (Section 3.2 and Fig. 10) lend support to the assumption insofar as a dimer formation is clearly observed for low coverages of isonicotinic acid.

The XAS results for a monolayer of isonicotinic acid are summarised in Fig. 8. We find quite similar results for the other molecules studied here. For an interpretation of the experimental data it has been assumed that the X-ray absorption measurements were performed on a well-ordered overlayer with a unit cell containing a two-molecule basis, similar to the adsorption geometry of benzoic acid on rutile $TiO_2(1\,1\,0)$ [32,33]. Each molecule is thus characterised by a set of angular parameters

Table 1
Amplitude ratios extracted from Figs. 4 and 5 and the counterparts for the nicotinic and picolinic acids

	Resonances A and B		Resonance D	
	$A(0°)/A(45°)$	$A(0°)/A(90°)$	$A(0°)/A(45°)$	$A(0°)/A(90°)$
Isonicotinic acid	0.60 ± 0.05	0.45 ± 0.05	0.7 ± 0.1	0.5 ± 0.1
Nicotinic acid	0.85 ± 0.05	0.62 ± 0.05	0.8 ± 0.1	0.9 ± 0.2
Picolinic acid	0.83 ± 0.07	0.43 ± 0.05		
Benzoic acid	0.80 ± 0.06	0.57 ± 0.05		

For picolinic acid we have only given the values for peak A since the intensity of peak D is forbiddingly small for a sensibly accurate quantification. In the case of benzoic acid the corresponding resonance is assumed to contain contributions from two excitations, D and H (see text), and has therefore been omitted here.

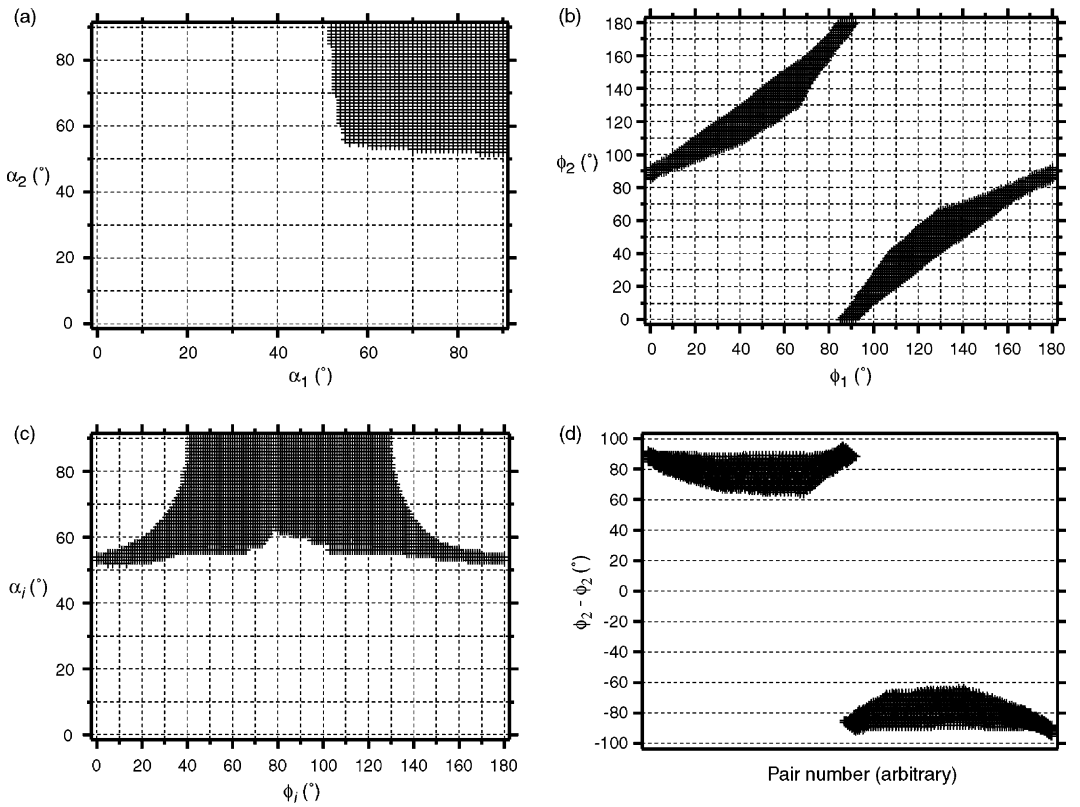

Fig. 8. Molecular angles compatible with the experimental X-ray absorption data for isonicotinic acid where a dimer geometry (i.e. two distinct molecular species) has been assumed. The crossed area represents allowed values, as described in the text. (a) Polar angle pair $\{\alpha_1, \alpha_2\}$. The polar angle of both molecules has to be larger than 50°. (b) Azimuthal angles $\{\phi_1, \phi_2\}$. (c) Possible azimuthal and polar angles for one of the two molecular species. Due to the symmetry of the assumption the result is the same for $\{\alpha_1, \phi_1\}$ and $\{\alpha_2, \phi_2\}$. (d) Difference between ϕ_1 and ϕ_2. Clearly, the difference between ϕ_1 and ϕ_2 has to amount to at least 60°, which is in favour of a 'T'-type geometry.

$\{\alpha_i, \phi_i\}$, where $i = 1, 2$ is the molecular index. The measured π^*-intensity is thus described by

$$I_{\text{total}} = I_1 + I_2,$$

in which the I_i take the form of Eq. (1). This assumption leads to the expression for the total amplitude $A(\omega) = A_1(\omega) + A_2(\omega)$ and a pair of ratios $\{A(0°)/A(45°), A(0°)/A(90°)\}$, now dependent on

four parameters $\alpha_1, \phi_1, \alpha_2, \phi_2$ instead of two as in the monomer case. Thus they cannot be uniquely determined as we only have two independent experimental amplitude ratios at hand. Instead, we investigated the four-dimensional parameter space in order to find out which parameters are consistent with the measurements. For that purpose we varied the parameters between 0° and 180° (ϕ_i) and 0° and 90° (α_i) in steps of 1°, calculated the amplitude ratios, and compared them to the experimental values ($A_{\mathrm{exp}}(0°)/\ A_{\mathrm{exp}}(45°) = 0.60 \pm 0.05$ and $A_{\mathrm{exp}}(0°)/A_{\mathrm{exp}}(90°) = 0.45 \pm 0.05$). Two-dimensional projections of sets of parameters $\{\alpha_1, \phi_1, \alpha_2, \phi_2\}$ whose amplitudes agree within the error margins given in Table 1 with the experimental values are displayed in Fig. 8. From these graphs we conclude that the molecular polar angle must be larger than 50° and that the azimuthal angles differ by 60–90°, i.e., the molecules arrange themselves in a 'T'-type fashion. We point out here, however, that these conclusions rely on the assumption of a dimer as opposed to a more complex geometry.

3.2. Scanning tunneling microscopy

In the STM experiments we investigated the isonicotinic acid/TiO_2(1 1 0) system with coverages that varied from the very-low coverage limit to nearly a full monolayer. Generally, only unoccupied substrate states were imaged. On clean TiO_2(1 1 0) mapping of the occupied states has thus far proved to be impossible [61], while we found that we were able to do so when the substrate was covered with molecules, although the tunneling conditions were less stable than when imaging the unoccupied states.

The degree of order of the overlayer depends strongly on the molecular partial pressure during sublimation. In cases of high partial pressures, 5×10^{-7} Torr in the doser volume before opening to the preparation chamber, the overlayer was not visibly well-ordered (Fig. 9), while we could achieve nicely ordered monolayers at doser volume pressures below 1×10^{-7} Torr. The substrate temperature probably also plays an important role, as we found a somewhat different X-ray absorption spectrum after dosing onto a sample

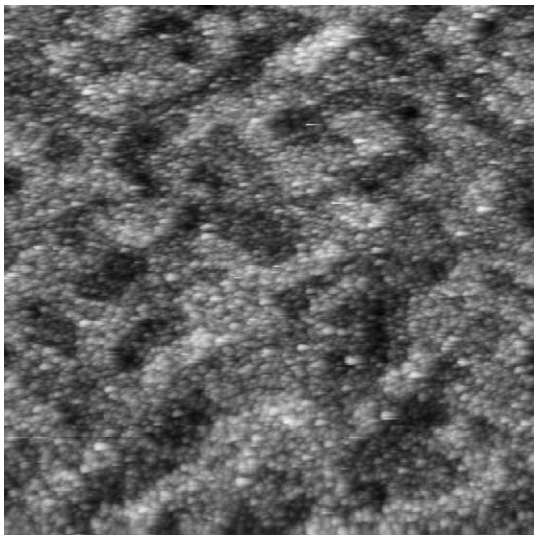

Fig. 9. 1500 Å × 1500 Å STM image (+2.8 V, 0.04 nA) after a "fast" evaporation of isonicotinic acid on TiO_2(1 1 0). The substrate terrace structure is visible as large brighter and darker regions. The adsorbate, however, does not seem to form an ordered overlayer. The surface is fully covered as was checked by alternating Auger electron spectroscopy measurements and further sublimations.

slightly higher in temperature (approximately 250 °C opposed to the usual 200 °C). In the following we will concentrate on the preparations using a low partial pressure, here referred to as preparations using a "slow" sublimation procedure.

In Figs. 10 and 11 samples with a coverage below 0.005 monolayers are imaged (a full monolayer is defined to contain one molecule per two substrate surface unit cells). Clearly visible are the alternating Ti and O rows of the substrate. The isonicotinic acid species are indicated by circles and arrows, respectively. The identification of these structures has been verified by adding a second small dosage. It can be observed that the molecules adsorb on the white rows, similar to the case of formic acid [63]. Most often the Ti atoms of TiO_2(1 1 0) samples are imaged as bright rows [61,64]. Since the benzoic acid species bind with the deprotonated carboxylic groups to the substrate Ti atoms (see part II), this finding is corroborated here.

A large percentage of the molecular species in the low-coverage preparation are contained in di-

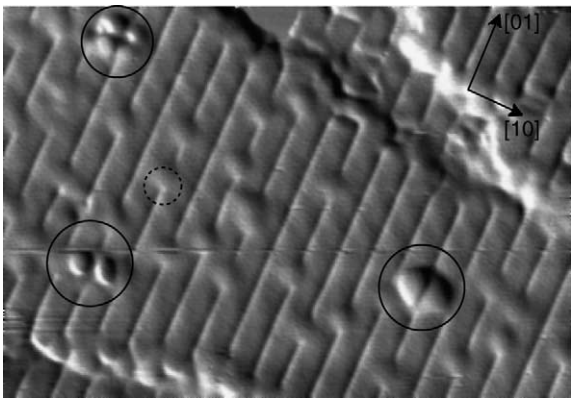

Fig. 10. 150 Å × 100 Å STM image of the preparation with the lowest coverage prepared in the series of experiments (+1.7 V, 0.09 nA). A differential was applied to the image in order to bring out the small details more clearly. [10] corresponds to [$\bar{1}$ 1 0] in bulk notation, and [0 1] to [0 0 1]. The isonicotinic acid adsorbates are marked by the solid circles, while the short-dashed circle indicates one of the oxygen vacancy defects. The defect appearance is a function of the tip mode [62], and from a clean crystal measurement we estimate that around 4% of the bridging oxygen atoms are missing. All the molecular species shown here form dimers (solid circles), and perhaps even a larger tetramer arrangement.

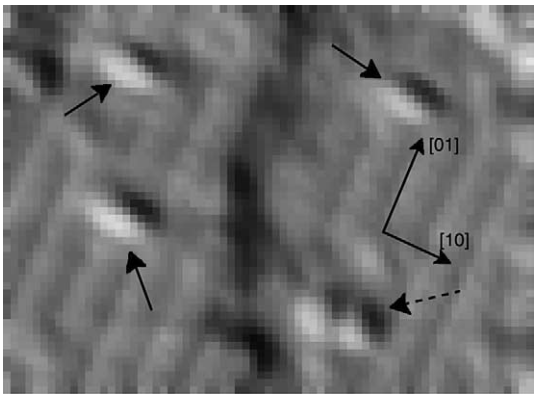

Fig. 11. 95 Å × 65 Å STM image (+1.7 V, 0.09 nA) of a low-coverage preparation of isonicotinic acid on TiO_2(1 1 0). The image was processed for a clearer presentation. Here, both monomers (solid arrows) and dimers (dashed arrow) are visible. From a larger scan not shown here it was found that approximately 75% of all molecules are bound in dimers or sometimes even larger arrangements.

mers and possibly even larger arrangements such as tetramers. The latter structure (cf. Fig. 10) can frequently be observed in the STM images, but we cannot entirely exclude a tip effect. From a scan not shown here it was found that around 75% of all molecules bind in dimer or larger arrangements.

In spite of the strong surface bond [39,65] and the corresponding STM observation that isonicotinic acid is not mobile at room temperature a nucleation into larger arrangements could principally be explained by some degree of molecular mobility on the surface at the elevated deposition temperature of 200 °C. For formic acid (HCOOH), which binds to the TiO_2(1 1 0) surface in the same dissociative carboxylic bidentate mode as isonicotinic acid, such a mobility has been observed at slightly elevated temperatures (ca. 50 °C) [66]. Interestingly, isolated molecules are not mobile. Onishi et al. [66] explained this behaviour by assuming a repulsive interaction between adjacent molecules. Käckell and Terakura [67] subsequently presented another explanation invoking a detailed diffusion mechanism. In this scheme, one of the Ti–molecule bonds is broken and the carboxyl group bonds doubly to a single Ti atom in a transition state. In this intermediate state the molecule is rotated with respect to its normal orientation and interacts strongly with the surrounding surface protons (originating from the dissociative adsorption of the acid), thereby substantially lowering the diffusion barrier. The rotation and associated proton–molecule interaction is not found for isolated molecules, and thus the experimental findings of Onishi et al. are explained in this picture. A similar mechanism could be imagined for isonicotinic acid. In contrast, a precursor state with a drastically different bond formation can be excluded, since pyridine, which interacts with the TiO_2(1 1 0) surface most strongly via its N-atom, has been found to desorb from the surface below room temperature [68]. This indicates that no such precursor geometry is available at the preparation temperature of 200 °C.

It should be pointed out that there is no 1:1 correspondence between the formate and isonicotinic acid cases. Experimentally it is found for formic acid that the overlayer becomes disordered at temperatures above 80 °C and the ordered array cannot be reproduced by recooling the sample, but an additional dosage of formic acid is required [69]. In contrast, we are able to produce an ordered isonicotinic acid overlayer at 200 °C, which

appears to point at an enhanced stability in comparison to formate. The ring–ring interactions suggested here and, especially, by the results of II provide a natural explanation of this, but at the same time would constitute a positive contribution to the diffusion probability.

Furthermore, it is likely that a large fraction of the molecules reach the surface already in the form of cyclic dimers (i.e., in an acid-to-acid geometry with two hydrogen bonds between the carboxylic groups; arguments for their existence in the gas phase are given below), for which, according to the interaction argument given above, the diffusion barrier would be enhanced compared to that of a monomer. For a landing geometry that is favourable for the formation of substrate bonds, the dimer would be adsorbed by establishing links between the carboxylic groups and the substrate Ti atoms (cf. paper II); otherwise the dimer would be rejected. Such a process would explain why larger arrangements than dimers are observed only to a very small extent for very low coverages, while approximately three quarters of all molecules are found in their dimer and about one quarter in their monomer form. Presently this explanation, however, leaves out a mechanism for the formation of relatively large fully packed domains in the monolayer as observed by STM.

It is known that carboxylic acids form cyclic dimers in the gas phase (see, e.g., [70,71]). While many of these molecules also form cyclic dimers in the bulk (see, e.g., [72,73]) the geometry of bulk isonicotinic acid is characterised by hydrogen bonds between the carboxylic group on one molecule and the nitrogen on the neighbouring molecule (head-to-tail geometry) [49,50,74] possibly further stabilised by weak C–H$\cdots$O hydrogen bonds [74]. We have tested these two competing gas phase geometries (head-to-tail and acid-to-acid) for isonicotinic acid in a dimer calculation. Both geometries are calculated to be more stable than the corresponding two-monomer situation, but the acid-to-acid one outweighs the head-to-tail one by 20 kJ/mol (the calculated stabilisation energy is 68 kJ/mol for the acid-to-acid geometry and 48 kJ/mol for the head-to-tail one). We propose therefore that the preferred gas phase geometry is that of a cyclic dimer.

The formation of these cyclic dimers in the gas phase has then to be explained by considering the sublimation process itself, since the vapour pressure of isonicotinic acid is too low (0.015 Pa at 362.15 K [75]) for a non-effusive flow in the Knudsen-cell like sublimator set-up required for a cooling by expansion. It has been observed previously that carboxylic acids evaporate from solution [76] and from clusters [77–79] in the form of cyclic dimers. Similarly to the explanation of Zhang and Lifshitz [79], who propose that formic acid dimers are evaporated from formic acid chains which contain dimers at the chain ends, we think that for isonicotinic acid the transition from the bulk head-to-tail situation to the gas phase acid-to-acid dimers could be explained by a surface effect in which dangling carboxylic groups occur, allowing neighbouring molecules to form acid-to-acid bonds.

It should be pointed out that the quantitative explanation of the exact mechanism of a dimer/cluster formation for low coverages, although interesting, is not fundamental for the conclusion that molecular interactions are important in the monolayer, as discussed for the XAS results above and in the following for high coverage STM images. The STM results below show that long-range ordering is the rule for the monolayers, and to a large extent for submonolayers. In II we show that pairs of dimers, i.e., tetramers, appear to be the fundamental unit for a complete monolayer, but the interactions within such units are easily extended to larger multiples of two. Thus the low coverage finding cannot give a full account of the more complicated monolayer interactions, but supports the notion that molecular interactions are of major importance for the exact adsorbate geometry, and opens the discussion of how ordered monolayer structures can form on a surface with which an individual molecule forms such a strong bond.

The ''slow'' high coverage preparations comprise a submonolayer (Fig. 12) and a full monolayer (Fig. 13). Both preparations show a considerable degree of ordering. In the submonolayer case a clear tendency of rows forming along [10] is observed, pointing to molecular interactions and enhanced adsorption probability in this direction. This

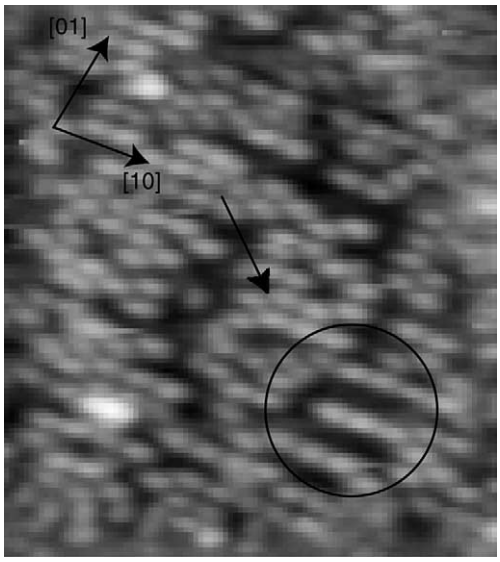

Fig. 12. 120 Å × 130 Å image of a "slow" submonolayer isonicotinic acid preparation obtained with a bias of +3.3 V and a tunnel current of 0.41 nA. The overlayer is clearly ordered with a conspicuous tendency of the molecules to form rows in the [10] direction. The circle marks a spot where the row-forming tendency is very pronounced. The finding supports the notion of a molecular interaction along [10]. The arrow indicates a spot at which the linear symmetry is broken and two adjacent molecules along [10] are shifted with respect to each other by half a net constant in the [0 1] direction. Similar shifts can be found for a monolayer, Fig. 13.

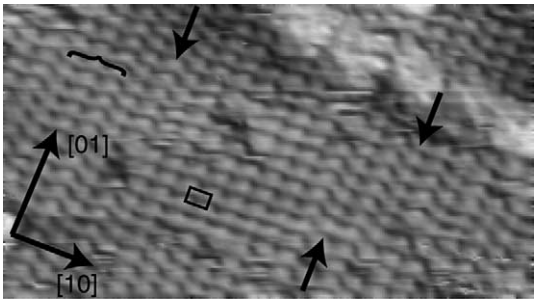

Fig. 13. 185 Å × 100 Å STM image (+2.4 V, 0.32 nA) of a monolayer preparation of isonicotinic acid on TiO_2(1 1 0) achieved by a "slow" evaporation. The image had a differential applied to bring out the small details. The substrate directions are indicated as well as the unit cell of the overlayer which has a (2×1)-structure. The arrows indicate rows which are shifted by half a net constant in the [0 1]-direction compared to adjacent rows. The curly bracket marks a three row-structure which could be the result of some degree of trimerisation.

suggests that the dimer formation in the low coverage limit has a counterpart in the high coverage regime, and that, in line with the discussion above, adsorbed molecules act as nucleation sites for continued adsorption. The full monolayer in Fig. 13 is ordered into a (2×1) overlayer structure. The molecules align nicely in the [0 1] as well as in the [10] direction.

3.3. Discussion

XPS [Paper II] and STM show that the basic adsorption parameters for the pyridinecarboxylic acids and benzoic acid on TiO_2(1 1 0) are in accordance with those of smaller carboxylic acids such as formic acid, namely that the binding occurs via the deprotonated carboxylic group to the fivefold-coordinated Ti atoms. Two surface unit cells can accomodate one molecule. The question of the ring orientation is more complicated. The XAS results show that all pyridinecarboxylic acid monomers and benzoic acid behave similarly in that regard. For a full monolayer, a pure monomer geometry with two equivalent ring plane orientations (two due to the twofold surface symmetry) can be excluded. Furthermore, the observation that the XAS intensity variation is dependent on the sample azimuth rules out a random orientation. In contrast, the data are fully compatible with dimer formation. Evidence for such a dimerisation is found in the low coverage STM on isonicotinic acid on TiO_2(1 1 0). Here, we find that dimer formation across the bridging oxygen rows is energetically favourable, although monomers are also stable at room temperature. Also for higher coverages a molecular ring interaction along [1 0] seems to be preferable. Similarly to the case of benzoic acid [32,33], some evidence of trimerisation can also be found in the STM image isonicotinic acid on TiO_2(1 1 0) of Fig. 13, as well as other structures not included in the dimer model, but these are not representative of the well-ordered overlayer.

What is clear is that the described behaviour can be rationalised from interactions between the rings of adjacent molecules, as proposed for benzoic acid [32,33]. The pyridine rings of the pyridinecarboxylic acids can be expected to interact

via van der Waals forces as do the phenyl rings of benzoic acid [32,33], and the polyphenylenes in bulk crystals, which form a well-known herringbone structure. An additional aspect in the present study is the presence of the nitrogen atom in the pyridine rings, which induces the formation of dipoles in their ground states, providing an electrostatic interaction when in close proximity. Considering a dimer, it is almost certain that the most favourable geometry will not be a plane-parallel one, although it is not straightforward to find the most stable geometry without proper potentials. That such an interaction is observed along the [1 0] vector of the substrate can be rationalised from the greater bending flexibility in this direction for a 2M-bidentate geometry. The situation is more complicated when modelling the monolayers. Here, one has to take into account the presence of several nearest and next-nearest neighbours as well as long-range electrostatic interactions. However, it seems very likely that a geometry that accomodates more than one ring orientation could stabilise the monolayer system substantially with respect to a single-species geometry, and this is discussed at greater length in II.

Spectroscopic evidence for such an interaction is found in the N 1s absorption spectra (Fig. 2). As outlined above, resonance C, which exhibits a σ^*-like angle dependence, is not reproduced by calculations of isolated or adsorbed molecules [80]. However, such calculations do not model the adsorbate interaction observed here. A pyridine ring interaction between two adjacent molecules accompanied by a tilt towards each other would favour an interaction of the N sp^2 lone pair orbital with a hydrogen atom of the neighbouring molecule. The observed intensity and its angle dependence can then be explained by a N–H like resonance similar to the C–H resonances in C 1s absorption spectra of hydrocarbons. Because of the steric hindrance to N-atom-neighbour-ring interactions constituted by the proximity of the N atom to the substrate-bound carboxylic group, we postulate that the formation of such a resonance is most probable for isonicotinic acid, less for nicotinic acid, and least for picolinic acid; this agrees well with the differing findings for the three pyridine-carboxylic acid molecules.

As noted above, the argument that intermolecular interactions determine the ring orientations is also valid for the non-polar benzoic acid [32,33]. Tsuzuki et al. [81] have proposed that the most stable geometry for a benzene dimer is T-shaped due to a combination of electrostatic and van der Waals-interactions. In their calculations a stabilisation energy of approximately 0.05 eV per molecule in a dimer has been found, which is approximately four times the thermal energy per degree of freedom. Thus, the experimental evidence for at least two different ring orientations (presented here and by Guo et al. [32,33]) agrees well with theoretical expectations, and can be expected to enhance pairing of molecules at low and high coverages, consistent with our observations.

4. Conclusions

The monolayer adsorption geometry of the pyridinecarboxylic acids and of benzoic acid on TiO_2(1 1 0) has been elucidated with the help of XAS and STM. The joint result of these techniques points at the importance of intermolecular interactions in the adsorption of these compounds. In the STM it is observed that the adsorption of isonicotinic acid is stabilised by dimer formation, and the XAS results suggest that this is true for the other molecules as well. The simplest structure compatible with the XAS and STM findings is one in which the molecules dimerise via ring interactions with an azimuthal orientational difference of 60–90°. Within this model, the ring planes are approximately perpendicular to the surface, with a polar angle of at most 40° from the surface normal. In a more general consideration, an investigation of the XAS intensities shows that the pyridine and phenyl ring orientation is neither random nor defined by a single set of molecular angles, i.e., there are at least two inequivalent molecular species. This result holds even if the dimer model should not be applicable. That a ring interaction has such a fundamental impact on the observed orientations is compatible with the expectation of strong electrostatic and van der Waals-interactions between the molecules.

Acknowledgements

We would like to acknowledge the staff at MAX-Lab for assistance in the experimental work, and our funding sources Vetenskapsrådet, the Consortium on Clusters and Ultrafine Particles, which is funded by Stiftelsen för Strategisk Forskning, and Göran Gustafssons Stiftelse. We would also like to thank H. Hillesheimer for help during the experiments and M. Odelius for stimulating discussions.

References

[1] W. Gerhartz (Ed.), Ullmann's Encyclopedia of Industrial Chemistry, VCH Verlagsgesellschaft, Weinheim, 1985.
[2] Y. Luo, D.F. Ollis, J. Catal. 163 (1996) 1.
[3] R. Méndez-Román, N. Cardona-Martinéz, Catal. Today 40 (1998) 353.
[4] L. Cao, Z. Gao, S.L. Suib, T.N. Obee, S.O. Hay, J.D. Freihaut, J. Catal. 196 (2001) 253.
[5] T. Yokoyama, T. Setoyama, N. Fujita, M. Nakajima, T. Maki, Appl. Catal. A 88 (1992) 149.
[6] J. Kondo, N. Ding, K. Maruya, T. Yokoyama, N. Fujita, T. Maki, Bull. Chem. Soc. Jpn. 66 (1993) 3085.
[7] Y. Sakata, C.A. van Tol-Koutstaal, V. Ponec, J. Catal. 169 (1997) 13.
[8] Y. Sakata, V. Ponec, Appl. Catal. A 166 (1998) 173.
[9] M.W. de Lange, J.G. van Ommen, L. Lefferts, Appl. Catal. A 220 (2001) 41.
[10] A. Hagfeldt, M. Grätzel, Acc. Chem. Res. 33 (2000) 269.
[11] M. Gfeller, G. Furrer, R. Schullin, Environ. Sci. Technol. 31 (1997) 3692.
[12] B.G. Frederick, M.R. Ashton, N.V. Richardson, T.S. Jones, Surf. Sci. 292 (1993) 33.
[13] P.D.A. Pudney, B.G. Frederick, N.V. Richardson, Surf. Sci. 307–309 (1994) 46.
[14] N.V. Richardson, B.G. Frederick, W.N. Unertl, A. El Farrash, Surf. Sci. 307–309 (1994) 124.
[15] J.E. Ivanecky III, C.M. Child, A. Campion, Surf. Sci. 325 (1995) L428.
[16] B.G. Frederick, F.M. Leibsle, S. Haq, N.V. Richardson, Surf. Rev. Lett. 3 (1996) 1523.
[17] T. Bitzer, T. Alkunshalie, N.V. Richardson, Surf. Sci. 368 (1996) 202.
[18] A. Schertel, C. Wöll, M. Grunze, J. Phys. IV 7 (1997) 537.
[19] B.G. Frederick, Q. Chen, F.M. Leibsle, M.B. Lee, K.J. Kitching, N.V. Richardson, Surf. Sci. 394 (1997) 1.
[20] B.G. Frederick, Q. Chen, F.M. Leibsle, S.S. Dhesi, N.V. Richardson, Surf. Sci. 394 (1997) 26.
[21] Q. Chen, B.G. Frederick, N.V. Richardson, J. Chem. Phys. 108 (1998) 5942.
[22] C.C. Perry, S. Haq, B.G. Frederick, N.V. Richardson, Surf. Sci. 409 (1998) 512.
[23] M. Neuber, M. Zharnikov, J. Walz, M. Grunze, Surf. Rev. Lett. 6 (1999) 53.
[24] M. Zharnikov, M. Neuber, M. Grunze, J. Elec. Spec. Rel. Phen. 99 (1999) 25.
[25] T. Bitzer, N.V. Richardson, Surf. Sci. 427–428 (1999) 369.
[26] M. Zharnikov, M. Neuber, Surf. Sci. 464 (2000) 8.
[27] Q. Chen, C.C. Perry, B.G. Frederick, P.W. Murray, S. Haq, N.V. Richardson, Surf. Sci. 446 (2000) 63.
[28] T. Bitzer, N.V. Richardson, S. Reiss, M. Wühn, C. Wöll, Surf. Sci. 458 (2000) 173.
[29] M. Pascal, C.L.A. Lamont, M. Kittel, J.T. Hoeft, R. Terborg, M. Polcik, J.H. Kang, R. Toomes, D.P. Woodruff, Surf. Sci. 492 (2001) 285.
[30] J.M. Vohs, M.A. Barteau, J. Phys. Chem. 93 (1989) 8343.
[31] S. Reynolds, D.P. Oxley, Surf. Sci. 368 (1996) 324.
[32] Q. Guo, I. Cocks, E.M. Williams, Surf. Sci. 393 (1997) 1.
[33] Q. Guo, E.M. Williams, Surf. Sci. 433 (1999) 322.
[34] C.A. Koutstaal, V. Ponec, Appl. Surf. Sci. 70–71 (1993) 206.
[35] K.D. Dobson, A.J. McQuillan, Spectrochim. Acta A 56 (2000) 557.
[36] L. Patthey, H. Rensmo, P. Persson, K. Westermark, L. Vayssieres, A. Stashans, Å. Petersson, P.A. Brühwiler, H. Siegbahn, S. Lunell, N. Mårtensson, J. Chem. Phys. 110 (1999) 5913.
[37] P. Persson, A. Stashans, R. Bergström, S. Lunell, Int. J. Quantum Chem. 70 (1998) 1055.
[38] P. Persson, S. Lunell, P.A. Brühwiler, J. Schnadt, S. Södergren, J.N. O'Shea, O. Karis, H. Siegbahn, N. Mårtensson, M. Bässler, L. Patthey, J. Chem. Phys. 112 (2000) 3945.
[39] J. Schnadt, P.A. Brühwiler, L. Patthey, J.N. O'Shea, S. Södergren, M. Odelius, R. Ahuja, O. Karis, M. Bässler, P. Persson, H. Siegbahn, S. Lunell, N. Mårtensson, Nature 418 (2002) 620.
[40] M. Odelius, P. Persson, S. Lunell, Surf. Sci. 529 (2003) 47.
[41] P. Persson, S. Lunell, Sol. Energy Mat. Solar Cells 63 (2000) 139.
[42] J. Schnadt, A. Henningsson, M.P. Andersson, P.G. Karlsson, P. Uvdal, H. Siegbahn, P.A. Brühwiler, A. Sandell, submitted to J. Phys. Chem. B.
[43] D.A. Stern, L. Laguren-Davidson, D.G. Frank, J.Y. Gui, C.-H. Lin, F. Lu, G.N. Salaita, N. Walton, D.C. Zapien, A.T. Hubbard, J. Am. Chem. Soc. 111 (1989) 877.
[44] A.T. Hubbard, J.Y. Gui, J. Chim. Phys. Phys. Chim. Biol. 88 (1991) 1547.
[45] S.M. Park, K. Kim, M.S. Kim, J. Mol. Struct. 328 (1994) 169.
[46] L.K. Noda, O. Sala, J. Mol. Struct. 162 (1987) 11.
[47] N.V. Nikolenko, Russ. J. Phys. Chem. 74 (2000) 2034.
[48] Y.G. Kim, S.L. Yan, K. Itaya, Langmuir 15 (1999) 7810.
[49] J.N. O'Shea, J. Schnadt, P.A. Brühwiler, H. Hillesheimer, N. Mårtensson, L. Patthey, J. Krempasky, C.K. Wang, Y. Luo, H. Ågren, J. Phys. Chem. B 105 (2001) 1917.
[50] J.N. O'Shea, Y. Luo, J. Schnadt, L. Patthey, H. Hillesheimer, J. Krempasky, D. Nordlund, M. Nagasano, P.A. Brühwiler, N. Mårtensson, Surf. Sci. 486 (2001) 157.

[51] J. Schnadt, J.N. O'Shea, L. Patthey, J. Schiessling, J. Krempasky, M. Shi, N. Mårtensson, P.A. Brühwiler, Surf. Sci., submitted.
[52] R. Denecke, P. Väterlein, M. Bässler, N. Wassdahl, S. Butorin, A. Nilsson, J.-E. Rubensson, J. Nordgren, N. Mårtensson, R. Nyholm, J. Elec. Spec. Rel. Phen. 101–103 (1999) 971.
[53] R. Nyholm, S. Svensson, J. Nordgren, A. Flodström, Nucl. Instrum. Meth. A 246 (1986) 267.
[54] J.N. Andersen, O. Björneholm, A. Sandell, R. Nyholm, J. Forsell, L. Thånell, A. Nilsson, N. Mårtensson, Synchr. Rad. News 4 (4) (1991) 15.
[55] Omicron Vakuumphysik GmbH, Taunusstein, Germany.
[56] J. Stöhr, NEXAFS Spectroscopy, Springer-Verlag, Heidelberg, 1992.
[57] J. Schnadt, J. Schiessling, J.N. O'Shea, L. Patthey, M. Shi, C. Puglia, N. Mårtensson, P.A. Brühwiler, Nucl. Instr. Meth. B 184 (2001) 609.
[58] M.J. Frisch, G.W. Trucks, H.B. Schlegel, G.E. Scuseria, M.A. Robb, J.R. Cheeseman, V.G. Zakrzewski, J.A. Montgomery Jr., R.E. Stratmann, J.C. Burant, S. Dapprich, J.M. Millam, A.D. Daniels, K.N. Kudin, M.C. Strain, O. Farkas, J. Tomasi, V. Barone, M. Cossi, R. Cammi, B. Mennucci, C. Pomelli, C. Adamo, S. Clifford, J. Ochterski, G.A. Petersson, P.Y. Ayala, Q. Cui, K. Morokuma, D.K. Malick, A.D. Rabuck, K. Raghavachari, J.B. Foresman, J. Cioslowski, J.V. Ortiz, A.G. Baboul, B.B. Stefanov, G. Liu, A. Liashenko, P. Piskorz, I. Komaromi, R. Gomperts, R.L. Martin, D.J. Fox, T. Keith, M.A. Al-Laham, C.Y. Peng, A. Nanayakkara, C. Gonzalez, M. Challacombe, P.M.W. Gill, B. Johnson, W. Chen, M.W. Wong, J.L. Andres, C. Gonzalez, M. Head-Gordon, E.S. Replogle, J.A. Pople, Gaussian 98, Revision A.7, Gaussian, Inc., Pittsburgh PA, 1998.
[59] W.H.E. Schwarz, T.C. Chang, U. Seeger, K.H. Hwang, Chem. Phys. 117 (1987) 73.
[60] C. Kolczewski, R. Püttner, O. Plashkevych, H. Ågren, V. Staemmler, M. Martins, G. Snell, A.S. Schlachter, M. Sant'Anna, G. Kaindl, L.G.M. Pettersson, J. Chem. Phys. 115 (2001) 6426.
[61] U. Diebold, J.F. Anderson, K.-O. Ng, D. Vanderbilt, Phys. Rev. Lett. 77 (1996) 1322, and references therein.
[62] U. Diebold, J. Lehman, T. Mahmoud, M. Kuhn, G. Leonardelli, W. Hebenstreit, M. Schmid, P. Varga, Surf. Sci. 411 (1998) 137.
[63] H. Onishi, Y. Iwasawa, Chem. Phys. Lett. 226 (1994) 111.
[64] C. Xu, X. Lai, G.W. Zajac, D.W. Goodman, Phys. Rev. B 56 (1997) 13464.
[65] J. Schnadt, J.N. O'Shea, L. Patthey, L. Kjeldgaard, J. Åhlund, K. Nilson, J. Schiessling, J. Krempaský, M. Shi, O. Karis, H. Siegbahn, N. Mårtensson, P.A. Brühwiler, submitted to J. Chem. Phys.
[66] H. Onishi, K. Fukui, Y. Iwasawa, Colloid Surf. A 109 (1996) 335.
[67] P. Käckell, K. Terakura, Surf. Sci. 461 (2000) 191.
[68] S. Suzuki, Y. Yamaguchi, H. Onishi, T. Sasaki, K. Fukui, Y. Iwasawa, J. Chem. Soc. Faraday Trans. 94 (1998) 161.
[69] H. Onishi, T. Aruga, C. Egawa, Y. Iwasawa, J. Catal. 146 (1994) 557.
[70] P.A. Kollman, L.C. Allen, Chem. Rev. 72 (1972) 283.
[71] S. Scheiner, Hydrogen Bonding: A Theoretical Perspective, Oxford University Press, New York, Oxford, 1997.
[72] L. Leiserowitz, Acta Crystallogr. Sect. B 32 (1976) 775.
[73] A.T. Dubis, S.J. Grabowski, D.B. Romanowska, T. Misiaszek, J. Leszczynski, J. Phys. Chem. A 106 (2002) 10613.
[74] F. Takusagawa, A. Shimada, Acta Cryst. B 32 (1976) 1925.
[75] R. Sabbah, S. Ider, Can. J. Chem. 77 (1999) 249.
[76] M. Faubel, T. Kisters, Nature 339 (1989) 527.
[77] W.Y. Feng, C. Lifshitz, J. Phys. Chem. 98 (1994) 6075.
[78] C. Lifshitz, W.Y. Feng, Int.J. Mass Spectrom. Ion Proc. 146–147 (1995) 223.
[79] R. Zhang, C. Lifshitz, J. Phys. Chem. 100 (1996) 960.
[80] M. Odelius, Private communication.
[81] S. Tsuzuki, K. Honda, T. Uchimaru, M. Mikami, K. Tanabe, J. Am. Chem. Soc. 124 (2001) 104.